NANO · MICRO small
www.small-journal.com

Boosting Cholesterol Efflux from Foam Cells by Sequential Administration of rHDL to Deliver MicroRNA and to Remove Cholesterol in a Triple-Cell 2D Atherosclerosis Model

*Shifa Jebari-Benslaiman, Kepa B. Uribe, Asier Benito-Vicente, Unai Galicia-Garcia, Asier Larrea-Sebal, Izortze Santin, Iraide Alloza, Koen Vandenbroeck, Helena Ostolaza, and César Martín**

Cardiovascular disease, the leading cause of mortality worldwide, is primarily caused by atherosclerosis, which is characterized by lipid and inflammatory cell accumulation in blood vessels and carotid intima thickening. Although disease management has improved significantly, new therapeutic strategies focused on accelerating atherosclerosis regression must be developed. Atherosclerosis models mimicking in vivo-like conditions provide essential information for research and new advances toward clinical application. New nanotechnology-based therapeutic opportunities have emerged with apoA-I nanoparticles (recombinant/reconstituted high-density lipoproteins, rHDL) as ideal carriers to deliver molecules and the discovery that microRNAs participate in atherosclerosis establishment and progression. Here, a therapeutic strategy to improve cholesterol efflux is developed based on a two-step administration of rHDL consisting of a first dose of antagomiR-33a-loaded rHDLs to induce adenosine triphosphate-binding cassette transporters A1 overexpression, followed by a second dose of 1,2-dipalmitoyl-sn-glycero-3-phosphocholine rHDLs, which efficiently remove cholesterol from foam cells. A triple-cell 2D-atheroma plaque model reflecting the cellular complexity of atherosclerosis is used to improve efficiency of the nanoparticles in promoting cholesterol efflux. The results show that sequential administration of rHDL potentiates cholesterol efflux indicating that this approach may be used in vivo to more efficiently target atherosclerotic lesions and improve prognosis of the disease.

1. Introduction

Cardiovascular disease (CVD), the leading cause of mortality in industrially developed countries,[1] is primarily caused by atherosclerosis, a progressive inflammatory disease of the arteries.[2–4] Atherosclerosis is characterized by an abnormal lipid and inflammatory cell accumulation in the intima, the subendothelial layer of large arteries.[5] During the development of atherosclerosis, several factors such as blood flow perturbation and hypercholesterolemia alter the function of both vascular endothelial cells (ECs) and smooth muscle cells (VSMCs), the main cellular components of arteries. These factors promote EC dysfunction and changes in VSMCs phenotype,[6,7] leading to vessel wall homeostasis perturbation and lipoprotein diffusion into the arterial wall.[8] Retention of cholesterol-rich lipoproteins in susceptible areas of the arterial vasculature favors low-density lipoprotein (LDL) oxidation, followed by endothelial activation, and macrophage infiltration, which internalize the modified LDL by a non-regulated mechanism leading to foam cell

S. Jebari-Benslaiman, A. Benito-Vicente, H. Ostolaza, C. Martín
Biofisika Institute (UPV/EHU
CSIC) and Department of Biochemistry and Molecular Biology
University of the Basque Country UPV/EHU
Leioa 48940, Spain
E-mail: cesar.martin@ehu.es

K. B. Uribe
Center for Cooperative Research in Biomaterials (CIC biomaGUNE)
Basque Research and Technology Alliance (BRTA)
San Sebastián 20014, Spain

The ORCID identification number(s) for the author(s) of this article can be found under https://doi.org/10.1002/smll.202105915.

DOI: 10.1002/smll.202105915

U. Galicia-Garcia, A. Larrea-Sebal
Fundación Biofisika Bizkaia and Biofisika Institute (UPV/EHU, CSIC)
Leioa 48940, Spain

I. Santin
Department of Biochemistry and Molecular biology
University of the Basque Country UPV/EHU
Leioa 48940, Spain

I. Santin, I. Alloza, K. Vandenbroeck
Biocruces Bizkaia Health Research Institute
Barakaldo 48903, Spain

I. Santin
CIBER (Centro de Investigación Biomédica en Red) de Diabetes y Enfermedades Metabólicas Asociadas (CIBERDEM)
Instituto de Salud Carlos III
Spain

differentiation.[9] As a result, atheroma plaque is developed and consequently, the vascular diameter is reduced thus increasing the incidence of cardiovascular events.[10–13]

The role of atherosclerosis as the major risk factor leading to cardiovascular complications[14,15] highlights the importance of finding new therapeutic strategies to facilitate the reverse of lipid build-up in the plaques. Cholesterol efflux from macrophages is a key process in reverse cholesterol transport (RCT) and promotes the delivery of excess cholesterol from peripheral cells and tissues to the liver for excretion.[16] RCT occurs through the interaction of apolipoprotein A-I (apoA-I) contained in high-density lipoproteins (HDL) with the adenosine triphosphate-binding cassette transporters A1/G1 (ABCA1/ABCG1).[17–19] Therefore, targeting RCT and ABCA1 could represent a valuable therapeutic approach to prevent atherosclerosis.

The inversely associated relationship between low HDL cholesterol levels and CVD risk in epidemiologic studies highlighted the potential of HDL mimetics (recombinant/reconstituted HDL or rHDL) as a therapeutic tool and inspirational source for biomedical engineering.[20–23] rHDL, designed to mimic the atheroprotective function of endogenous pre-β HDL particles, are complexes of full-length apoA-I or apoA-I mimetic peptides and phospholipids. Their characteristics allow rapid mobilization of cholesterol from periphery to plasma and have shown to reduce atherosclerosis burden in animal models.[24–28]

Based on these encouraging data, several rHDL have been designed and used in clinical trials for CVD therapy.[20,29] The discovery of apoA-I Milano, a natural apoA-I variant associated with very low levels of HDL and reduced atherosclerosis,[30,31] allowed formulating ETC-216. This rHDL is composed of apoA-I-Milano and phospholipids that mimics the properties of nascent HDL. In the phase II "The ApoA-I Milano Trial," ETC-216 showed a mean 2.7% coronary atherosclerosis regression in acute coronary syndrome patients but also development of serious adverse effects in some patients thus its use was discontinued.[32] A new formulation containing apoA-I-Milano, denominated MDCO-216, was tested and proven to be safe in terms of immunostimulatory effects.[33] However, the phase I/II MILANO-Lipids, and Other Surrogate Biomarkers Trial (PILOT) study and the second phase II trial, MILANO-DRIVE demonstrated its lack of efficacy.[34]

Another rHDL with ability to rapidly mobilize large amounts of cholesterol into the HDL fraction is CER-001. This rHDL is composed of recombinant human apoA-I and a lipid mixture composed of sphingomyelin and 1,2-dipalmitoyl-sn-glycero-3-phospho-(1′-rac-glycerol). Although CER-001 did not cause any significant reduction in coronary atherosclerosis as evaluated in the CHI-SQUARE study,[35] it has been shown a U-shaped CER-001 dose-response curve with the greatest atheroma regression occurring at a low concentration.[35]

Finally, CSL-112 is a rHDL consisting of human plasma derived apoA-I and soybean phosphatidylcholine (apoA-I : lipid, mol ratio = 1 : 55), which arose as an improvement of its predecessor, CSL-111. CSL-111 initially showed an enhanced cholesterol mobilization and improved anti-inflammatory markers, but was disfavored due to its hepatotoxicity.[36] On the contrary, CSL-112 was well tolerated and not associated with any significant alterations in liver or kidney function.[21] Moreover, CSL-112 has been found to enhance cholesterol efflux very efficiently[37] and its beneficial potential in reducing major adverse cardiovascular events will be assessed in the on-going large phase III AEGIS-II study (NCT03473223).[21,29]

Importantly, the physicochemical characteristics of rHDLs should be taken into consideration to improve their efficiency on promoting cholesterol efflux.[38,39]. Very recently, the efficiency of cholesterol removal by rHDL mimicking different HDL maturation stages has shown to be higher with 1,2-dipalmitoyl-sn-glycero-3-phosphocholine (DPPC) rHDL, a nanoparticle that resembles nascent HDL. In fact, cholesterol efflux from macrophage- and vascular smooth cell-derived foam cells induced by DPPC rHDL was even more efficient than that induced by rHDL with the lipid composition of CSL-112. Among the physicochemical characteristics of DPPC rHDL underlying this effect are the higher physical binding affinity of cholesterol for saturated long-chain-length phospholipids and the planar geometry of the DPPC lipid bilayer, which favors cholesterol transfer.[38–40] In addition, it has been shown that cholesterol transfer to DPPC rHDLs, which show a planar bilayer, is favored thermodynamically from the high curvature of the cell membrane promoted by ABCA.[40,41]

Therefore, the use of well-formulated apoA-I nanoparticles constitutes a significant advance toward clinical application because at therapeutic doses they neither present toxicity nor immunogenicity, making them appropriate for therapeutic application.[42] Based on their biocompatibility, rHDL can be considered ideal carriers for the delivery of drugs and other therapeutic agents, as it has been shown for DNA and synthetic RNA, when incorporating cationic or zwitterionic lipids within rHDLs.[43,44]

The discovery that multiple miRNAs participate in the progression of atherosclerosis and in the regulation of RCT by directly targeting ABCA1 has opened new opportunities in the use of nanotechnology-based miRNAs therapeutic platforms.[45,46] One of the most studied and well-known "target" of ABCA1 is miR-33a. As an intronic miRNA, miR-33a expression is linked to that of SREBP2 and both co-ordinately participate in the regulation of intracellular cholesterol levels.[47] Among the multiple roles in the regulation of cholesterol metabolism, miR-33a functionally regulates the activity of ABCA1 interfering with the protein expression. Both therapeutic and macrophage-specific miR-33 knockdown intervention to reduce miR-33 levels provided promising results in the past.[47] The advantages of using miRNAs rely both on their small repressive capacity on any single target gene, which is usually less than twofold and on their inherent ability to target multiple genes in the same biological pathway.[48,49] It has been shown that the inhibition of miRNAs using antisense oligonucleotides promotes RCT through upregulation of the *ABCA1* gene.[45,46] Therefore, some studies have used cationic lipid/polymer-based nanoparticles for miRNA delivery in preclinical models,[50] while some others have delivered functional miRNA mimics into macrophages in chitosan nanoparticles to promote RCT in vivo.[51] Nguyen et al. showed that miR-33 can be delivered to naïve macrophages by chitosan nanoparticles and modulates the expression of its target gene, *ABCA1*, both in vitro and in vivo and have suggested that these miRNA containing nanoparticles can be used in vivo to target atherosclerotic lesions.[51]

Given the huge complexity of atherosclerotic disease, the use of coculture systems reflecting the cellular complexity of atherosclerosis has been identified as an advantageous approach to in vitro research.[52] The importance of these in vitro studies relies on i) the demand to overcome the translational gap, ii) provide a suitable model to understand the physiological mechanisms underlying RCT, and iii) improve the efficiency of the nanoparticles in promoting cholesterol efflux, functional pathways that are central to the development of atherosclerosis.

In that context, in this work we sought to develop a therapeutic strategy to improve RCT and cholesterol efflux based in a two-step administration of rHDL (**Figure 1**). In a first nanodisc administration, antagomiR-33a-loaded DPPC:cholesteryl ester (CE):1-palmitoyl-2-hydroxy-sn-glycero-3-phosphocholine (LPC) rHDLs have been used to induce the overexpression of ABCA1 transporter, and in a second step, DPPC rHDLs have been used to remove more efficiently cholesterol from foam cells. A triple-compartment cell culture 2D model comprising ECs, SMCs and foam cells has been used mimicking the atheroma plaque components in vitro.[53] This strategy allows independent isolation of each cellular compartment for downstream analysis without cell sorting.

We find that sequential administration of rHDL potentiates cholesterol efflux compared to one-step administration of DPPC rHDL. The results indicate that delivery of antagomiR-33a by rHDL efficiently upregulates ABCA1 expression and potentiates the cholesterol efflux induced by DPPC rHDL from foam cells in a 2D atheroma model. Overall, these data indicate that this therapeutic approach might be used in vivo to target more efficiently atherosclerotic lesions and improve prognosis of the disease.

2. Results

2.1. Development and Biophysical Characterization of DPPC:CE:LPC and DPPC rHDL

HDL were reconstituted with DPPC:CE:LPC (75:20:5% mol) for antagomiR-33a delivery or DPPC alone for cholesterol efflux as indicated in the Experimental Section. ApoA-I:lipid ratio was optimized to 1:125 mol:mol in both compositions. Nanoparticle formation is illustrated in **Figure 2**A. Once reconstituted, rHDLs were purified by size exclusion chromatography. As shown in Figure 2B, rHDL showed a homogeneous peak centered at 11–13 mL, preceding the elution of free apoA-I at 15 mL. Size distribution of nanodiscs determined by dynamic light scattering (DLS) showed an average diameter of the

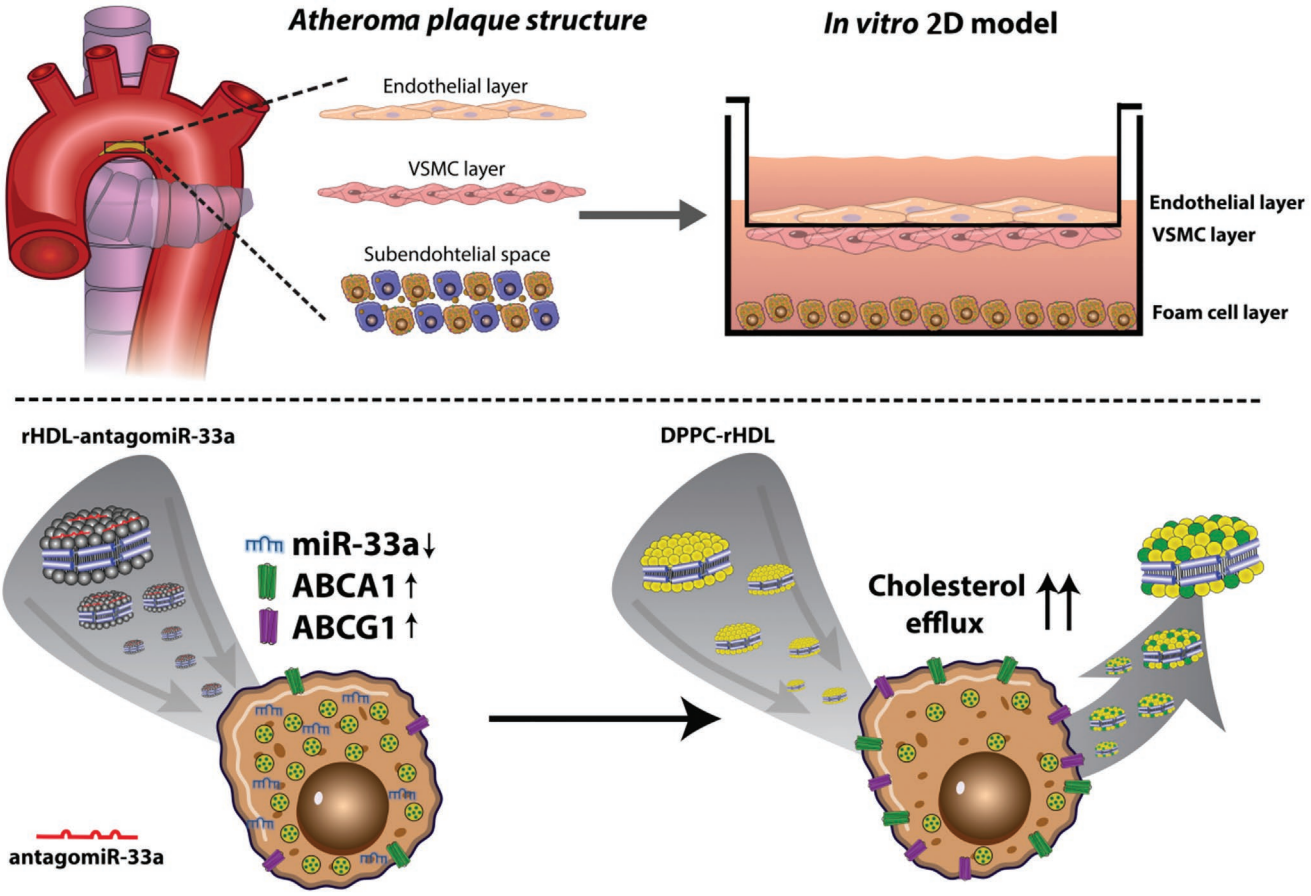

Figure 1. Schematic representation of the strategy to improve RCT and cholesterol efflux based in a two-step administration of rHDL. Overexpression of ABCA1 transporter is induced by a first administration with antagomiR-33a-loaded DPPC:CE:LPC rHDLs. A second step, which involves DPPC rHDLs administration, is used to remove more efficiently cholesterol from foam cells.

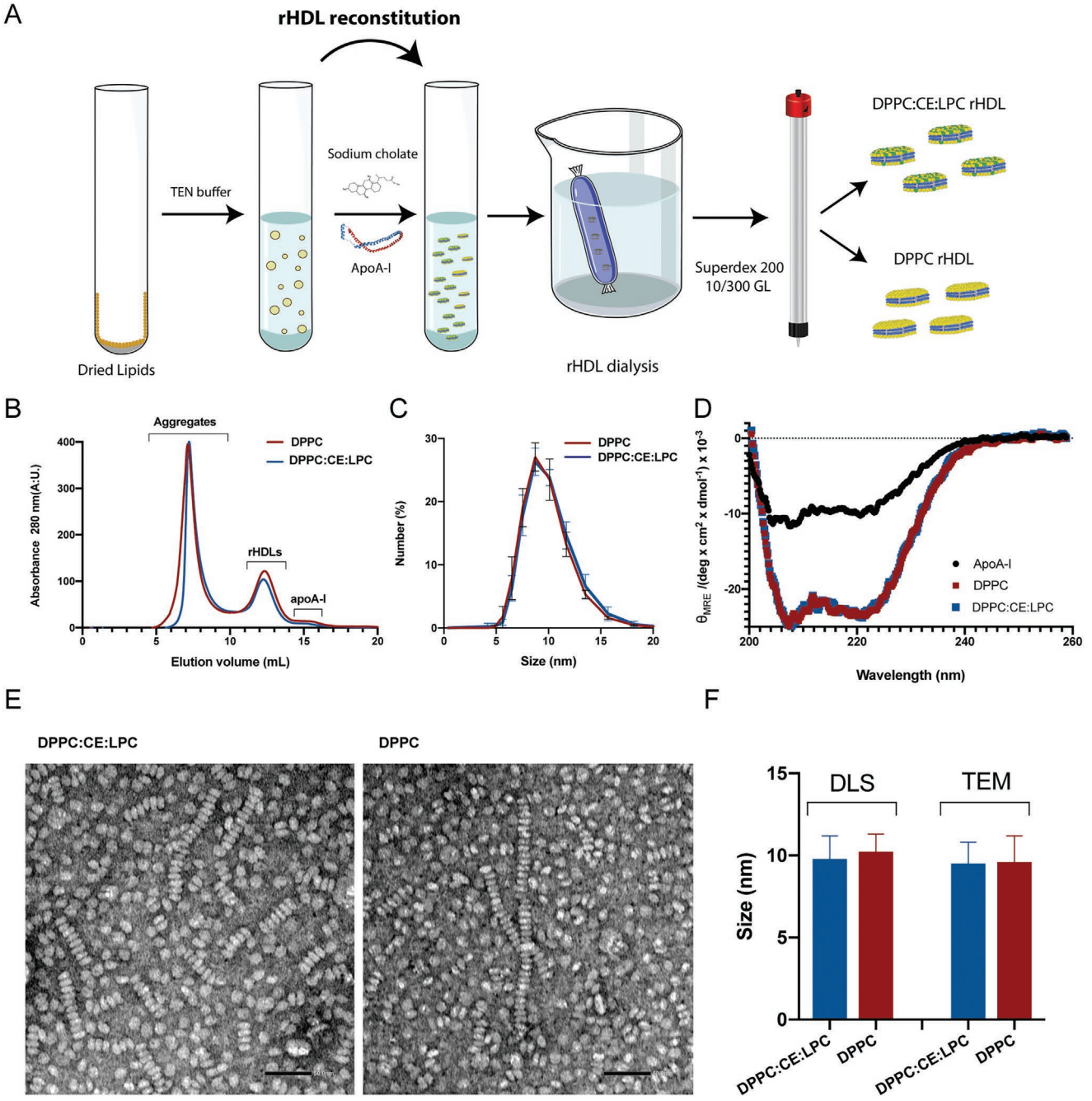

Figure 2. Development and biophysical characterization of rHDL. A) Schematic representation of rHDL reconstitution and purification by gel filtration chromatography on a Superdex 200 column. B) Gel filtration profiles of DPPC and DPPC:CE:LPC rHDLs, profiles were monitored by absorbance at 280 nm. C) rHDL size profiles determined by DLS. No significant differences between the different rHDL compositions were determined. D) Circular dichroism of DPPC and DPPC:CE:LPC rHDLs and apoA-I protein in solution. θ_{MRE}: mean residue ellipticity. E) Representative rHDL transmission electron microscopy images. Magnification 100×. Scale bar of 50 nm. F) rHDL diameter determined from DLS (hydrodynamic diameter) and NS-EM images. Size of rHDL (F) was measured as Feret diameter calculated from 1600 particles.

particles of ≈10 nm (Figure 2C,F). Finally, α-helical structure content determined by circular dichroism (CD) showed higher α-helical content in rHDLs compared to free apoA-I (≈2.2–2.5 times, Figure 2D and **Table 1**). These results indicate a correct reconstitution of rHDLs (Figure 2B–D). Size and morphology of nanoparticles were determined by negative stain electron microscopy (NS-EM) (Figure 2E), which showed a circular morphology, consistent with a discoid shape as shown by typically stacked nanoparticles resembling a "rouleaux" formation and, circular shapes presented by nanodiscs viewed from the top (Figure 2E). Longitudinal and transverse axes were 10.6 ± 0.8 and 3.9 ± 0.4 nm, respectively. The longitudinal axis

Table 1. α-helical content of apoA-I and rHDL determined by CD.

	α-Helical content	α-Helicity ratio rHDL/apoA-I
apoA-I	31.1 ± 2.0	–
DPPC	71.3 ± 2.5[a)]	2.3 ± 0.2[a)]
DPPC:CE:LPC	67.4 ± 3.4[a)]	2.2 ± 0.1[a)]

[a)]α-helical content calculated from ellipticity values measured at 222 nm. *R* is the ratio of α-helicities between rHDLs and free protein. Data represent the mean ± SD (n = 3). All measurements were performed independently three times and levels of significance were determined by a two-tailed Student's *t*-test. * $p < 0.01$ compared to apoA-I.

was similar to the diameter range (8–10 nm) determined by both DLS and NS-EM (Figure 2F).

2.2. Binding of miRNA to rHDL

Next, DPPC:CE:LPC rHDL particles were loaded with a control miRNA as illustrated in **Figure 3**A. Binding efficiency of miRNA was assessed at different miRNA:apoA-I ratios. As shown in Figure 3B, maximum miRNA binding was obtained at 1:1 mol:mol ratio.

2.3. Delivery of AntagomiR-33a by DPPC:CE:LPC rHDL into Foam Cells in Atheroma Plaque Model

2.3.1. 2D Atheroma Plaque Model Setup

A modular coculture system, which facilitates the separation of each cellular compartment, was used to set up a three-cell 2D-atheroma model. The system allows coculturing ECs, VSMCs, and macrophage-derived foam cells mimicking the vascular compartment thus facilitating the study of dynamics and interaction of rHDL with foam cells. A schematic illustration of the model is shown in **Figure 4**A. The use of 0.4 µm pored transwell inserts allows separation of VSMCs and ECs by a thin transwell membrane. This avoids translayer contamination by the other cell types while at the same time allows to individually isolate each culture layer. Barrier function was validated by determining transendothelial electrical resistance (TEER) of ECs. The calculated TEER value calculated by Ohm's law, 24.6 ± 1.2 Ω cm^2 confirmed integrity and permeability of the in vitro barrier and are in agreement with values reported by others.[54,55]

As illustrated in Figure 4B, delivery of antagomiR-33a by DPPC:CE:LPC rHDL would promote miR-33a silencing and consequently upregulation of ABCA1 and ABCG1 transporters.

2.3.2. Uptake of DPPC:CE:LPC rHDL by ECs, VSMC, and Foam Cells

We next aimed to address the delivery of antagomiR-33a by rHDL through the 2D atheroma model and determined the efficiency of rHDL uptake by ECs, VSMCs and foam cells in confluent populations. To establish the optimal condition for efficient microRNA delivery, different concentrations of rHDL were used (0–100 µg mL^{-1}) (Figure 4C) and uptake of DiI-labeled DPPC:CE:LPC rHDL by the different cell types was assessed after 24 h by fluorescent microscopy and flow cytometry. As shown in Figure 4, foam cells were extremely avid internalizing DPPC:CE:LPC rHDL (Figure 4C, lower panel). On the other hand, VSMCs showed residual rHDL uptake (Figure 4C, middle panel) while ECs internalized rHDL in a moderate way (Figure 4C, top panel) compared to foam cells. To quantify rHDL uptake efficiency, cells from the different compartments were isolated after incubation with the nanoparticles and their uptake was analyzed by flow cytometry as described in the Experimental Section. As shown in

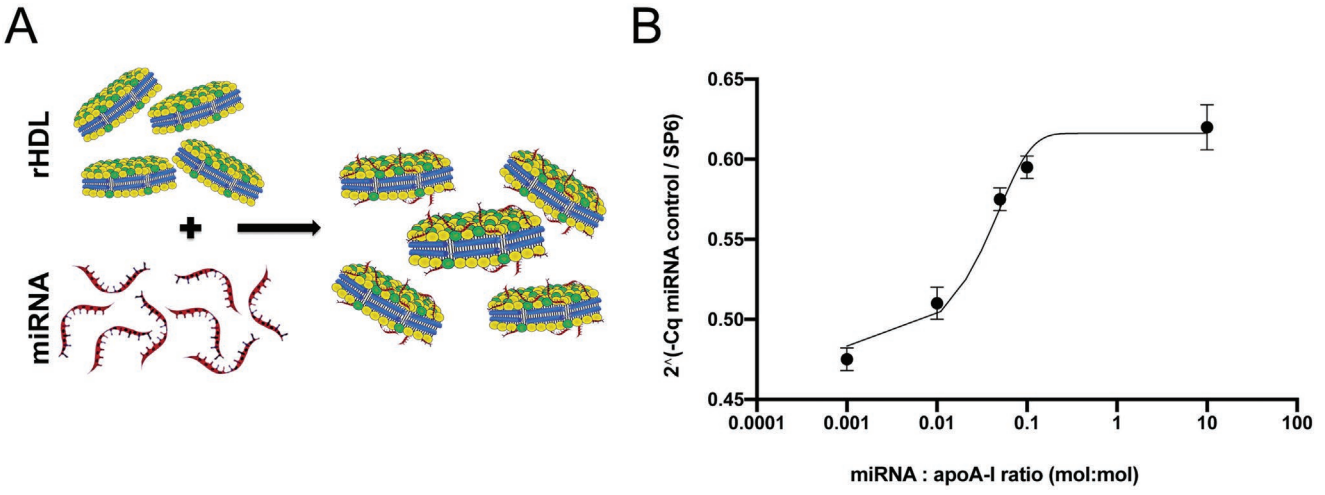

Figure 3. MicroRNA loading of DPPC:CE:LPC rHDL. A) Schematic representation of rHDL loading with microRNA. B) Efficiency of miRNA binding to rHDL determined by qRT-PCR. A mimic control (cel-miR-67 mature sequence) was used at miRNA:protein mol ratios ranging 0.001–10:1. Binding efficiency was calculated as described in the Experimental Section. Data represent the mean ± SD of at least three independent measurements.

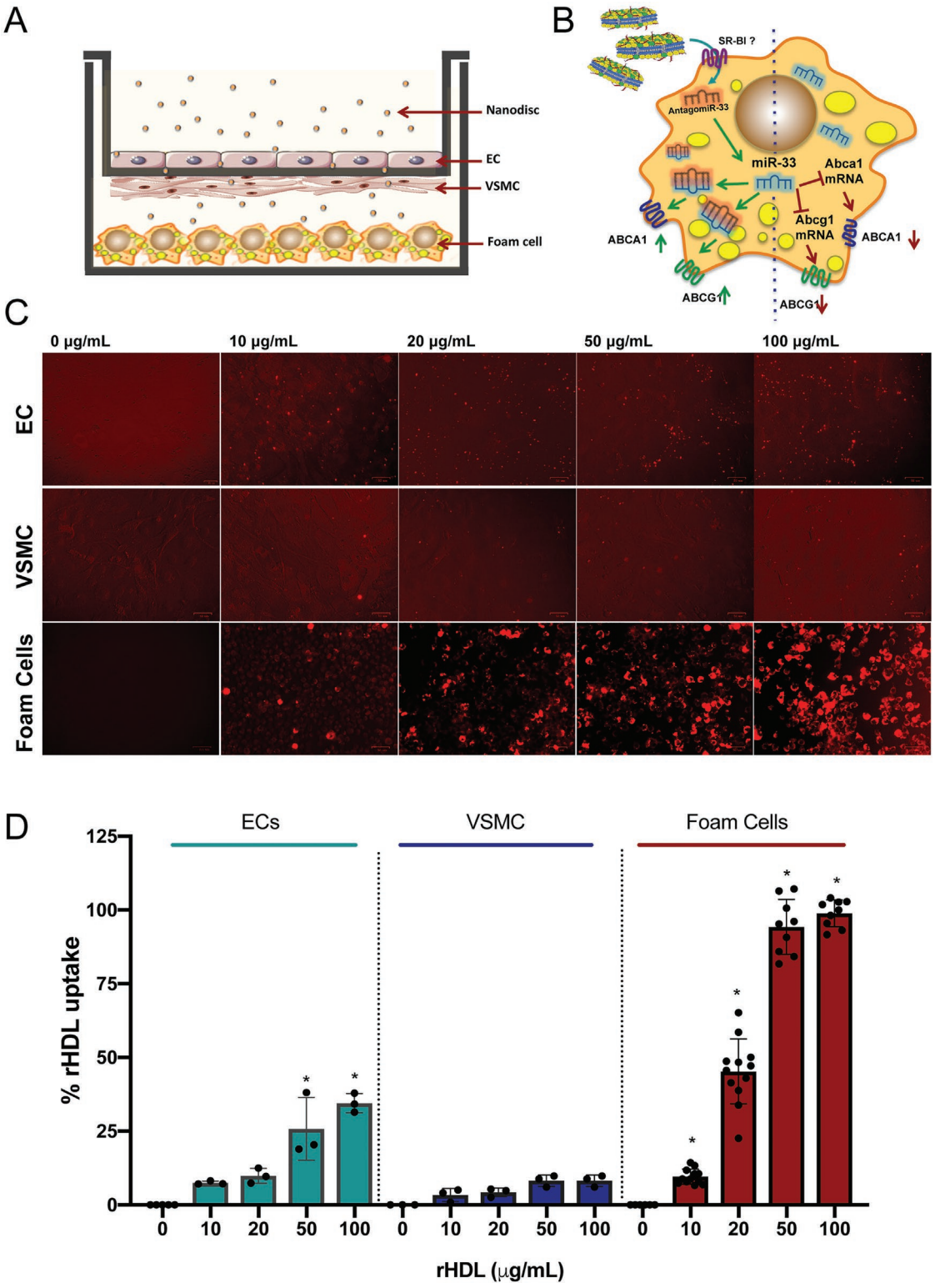

Figure 4. DPPC:CE:LPC rHDL are efficiently delivered into foam cells in the 2D atheroma model. A) A schematic illustration of the 2D atheroma model. The system allows coculturing ECs, VSMCs, and macrophage-derived foam cells mimicking the vascular compartment. B) ABCA1 and ABCG1 upregulation in foam cells by the delivery of antagomiR-33a loaded rHDL, which promotes miR-33a silencing. C) Fluorescent images showing rHDL uptake in ECs (top panel), VSMC (middle panel), and foam cells (lower panel) at different rHDL concentrations (0–100 µg mL^{-1}). D) Uptake of DiI-labeled DPPC:CE:LPC rHDL concentrations (0–100 µg mL^{-1}) by the different cell types assessed by flow cytometry. Data represent the mean ± SD of at least three independent measurements. Levels of significance were determined by a two-tailed Student's *t*-test. * $p < 0.01$ compared to no rHDL addition (0 µg mL^{-1}). Scale bars 50 µm.

Figure 4D, and confirming the results obtained by fluorescent microscopy, foam cells showed the highest ability in rHDL uptake, which resulted saturated at 50 μg mL^{-1}. Considering the fluorescence determined in foam cell uptake when treated with 100 μg mL^{-1} as 100%, rHDL uptake by ECs was 34% compared to foam cells while the uptake by VSMCs resulted residual (Figure 4D).

2.3.3. Delivery of AntagomiR-33a by DPPC:CE:LPC rHDL to Foam Cells

Intracellular delivery of miRNA by rHDL to foam cells was then assessed in the 2D atheroma model. First, delivery of cel-miR-67 (a microRNA that is naturally and specifically expressed in *C. elegans*) was used to set up validation. DPPC:CE:LPC rHDL particles loaded with cel-miR-67 at 1:1 mol:mol ratio were added in the ECs compartment at different concentrations (0–100 μg mL^{-1} rHDL) and miRNA incorporation into foam cells was determined after 24 h incubation with nanoparticles (**Figure 5**A). Total RNA was purified and intracellular cel-miR-67 levels were quantified as indicated in the Experimental Section. As shown in Figure 5A, delivery efficiency of miRNA reached maximum values at 100 μg mL^{-1} rHDL.

Similarly, a DPPC:CE:LPC rHDL dose-dependent (0–20 μg mL^{-1} rHDL) uptake assay was performed in macrophage-derived foam cells cultured alone in monolayer. In the absence of the vascular barrier simulated in the 2D atheroma model, the rHDL concentration required to achieve maximal delivery resulted five times lower (10 μg mL^{-1} rHDL) compared with the ones required in the 2D atheroma model (Figure S1, Supporting Information).

We next examined the ability of silencing miR-33a by delivering antagomiR-33a in DPPC:CE:LPC rHDL in the 2D atheroma model. Therefore, nanoparticles were loaded with antagomiR-33a and then, 50 μg mL^{-1} rHDL-antagomiR-33a were added into the ECs compartment and incubated for 48 h. Delivery of antagomiR-33a to foam cells by rHDL reduced approximately four times the levels of endogenous miR-33a compared with cells treated with nanodisc carrying control miRNA (Figure 5B). The extent of miR-33a silencing was also analyzed by determining the mRNA levels of ABCA1 and ABCG1, two known targets of miR-33a. As shown in Figure 5C, treatment with antagomiR-33a loaded rHDL resulted in ≈2.5- and twofold higher levels of ABCA1 and ABCG1 compared to control cells (treated with control miRNA), respectively. Similarly, upregulation of ABCA1 and ABCG1 protein levels in foam cells by delivering antagomiR-33a in DPPC:CE:LPC rHDL was confirmed by

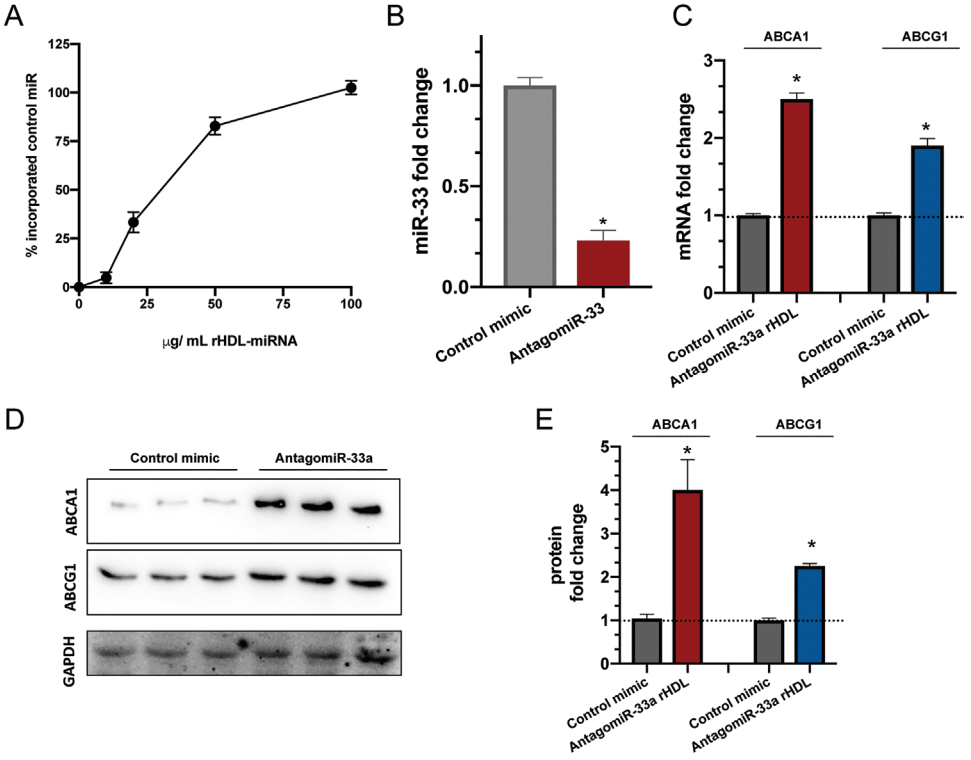

Figure 5. miRNA transfer capacity, miR-33a downregulation, and ABCA1/ABCG1 upregulation by miRNA delivery by DPPC:CE:LPC rHDL to foam cells. rHDLs were added to the cells in Opti-MEM to allow miRNA delivery, mir-33a repression, and protein upregulation. A) Intracellular delivery of miRNA by rHDL to foam cells assessed in the 2D atheroma model. DPPC:CE:LPC rHDL particles loaded with cel-miR-67 at 1:1 mol:mol ratio were added in the ECs compartment at different concentrations (0–100 μg mL^{-1} rHDL). B) miR-33a silencing by delivering antagomiR-33a in DPPC:CE:LPC rHDL (50 μg mL^{-1}) in the 2D atheroma model. C) mRNA levels of ABCA1 and ABCG1 after delivery of antagomiR-33a by rHDL to foam cells. MiR-33a and mRNA levels were determined after incubation of rHDL with 2D atheroma model foam cells during 48 h by qRT-PCR determined as described in the Experimental Section. D) Upregulation of ABCA1 and ABCG1 protein levels in foam cells by delivering antagomiR-33a in DPPC:CE:LPC rHDL. E) Expression levels of ABCA1 and ABCG1 determined by optical density. The data in (A), (B), (C), and (E) represent the mean ± SD of at least three independent measurements. The data in (D) correspond to a representative western blot of $n = 3$. Levels of significance were determined by a two-tailed Student's *t*-test. *$p < 0.01$ compared to control miRNA.

Western blot Figure 5D. Expression levels of ABCA1 and ABCG1 determined by optical density were 4.0 ± 0.8 and 2.3 ± 0.6, respectively (Figure 5E).

2.4. Cholesterol Efflux Promoted in Foam Cells within the 2D Atheroma Model

Finally, the efficiency of cholesterol efflux induced by sequential administration of antagomiR-33a by DPPC:CE:LPC rHDL followed by DPPC rHDL was evaluated in macrophage-derived foam cells loaded with TopFluor Cholesterol (**Figure 6**A).[56] The efficiency of DPPC rHDL as cholesterol acceptor was compared with natural HDL (Figure 6B).

Additionally, a comparative study between cholesterol efflux in foam cells cultured in 1D and foam cells grown in the 2D atheroma model was performed. AntagomiR-33a-loaded DPPC:CE:LPC rHDL at 10 μg mL^{-1} was used in foam cells cultured alone and, 50 μg mL^{-1} in the 2D atheroma model. Nanoparticles were incubated for 48 h with the cells to allow cargo delivery and ABCA1/ABCG1 upregulation. After cholesterol loading, DPPC rHDL (10 μg mL^{-1}) or HDL (10 μg mL^{-1}) were administered and incubated for 6 h to allow cholesterol efflux (Figure 6C).

2.4.1. HDL as Cholesterol Acceptor

Incubation with miRNA-devoid rHDL (empty-rHDL) induced a cholesterol efflux to HDL of ≈5% in both 1D and 2D atheroma model cultured foam cells (Figure 6D). The contribution of upregulating ABCA1 and ABCG1 to cholesterol efflux was assessed by incubating the cells with TO901317, an LIVER X RECEPTOR (LXR) agonist, as an internal control of the assay.[57] As shown in Figure 6D, TO901317 treatment increased significantly cholesterol efflux to HDL when compared to cells treated with empty-rHDL in both 1D and 2D cultured foam cells (Figure 6D). Similarly, upregulation of ABCA1 and ABCG1 by delivery of antagomiR-33a promoted a significant enhancement of cholesterol efflux to HDL. On the other hand, treatment with TO901317 and antagomiR-33a in combination caused a three times higher cholesterol efflux compared to cells treated with empty-rHDL (Figure 6D). Combination of TO901317 and antagomiR-33a-rHDL caused a synergistic upregulation of ABCA1 and ABCG1 protein levels in foam cells (Figure S2, Supporting Information).

The cholesterol efflux was paralleled by a similar reduction in the intracellular cholesterol content (Figure S3A, Supporting Information).

2.4.2. DPPC rHDL as Cholesterol Acceptor

DPPC as cholesterol acceptor showed a higher efficiency in terms of cholesterol efflux compared to HDL (Figure 6E). Treatment with DPPC:CE:LPC rHDL without antagomiR-33a (10 μg mL^{-1} rHDL in 1D or 50 μg mL^{-1} rHDL in the 2D atheroma model) induced a cholesterol efflux of ≈7.5% in both 1D cultured foam cells and 2D cultures (Figure 6E). Stimulation of LXR with TO901317 resulted in a significantly increased cholesterol efflux of 52 and 59% in 1D and 2D cultured foam cells, respectively, compared to cells treated with rHDL without antagomiR-33a (7.3 ± 1.5 vs 11.1 ± 1.3, and 8.3 ± 1.8 vs 13.2 ± 0.6, respectively) (Figure 6E). Delivery of antagomiR-33a by DPPC:CE:LPC rHDL into foam cells (10 μg mL^{-1} rHDL in 1D or 50 μg mL^{-1} rHDL in the 2D atheroma model) increased cholesterol efflux by 100 and 77% in 1D and 2D cultured foam cells, respectively (7.3 ± 1.5 vs 14.6 ± 0.8 and 8.3 ± 1.8 vs 14.7 ± 1.2, respectively). On the other hand, treatment combination with TO901317 and antagomiR-33a also caused a higher effect on cholesterol efflux than cells treated with the agonist and antagomiR-33a alone (Figure 6E). The reduction in the intracellular cholesterol content when DPPC rHDL was used as cholesterol acceptor paralleled the cholesterol efflux to rHDL (Figure S3B, Supporting Information). In addition, data indicate that five times higher concentrations of antagomiR-33a loaded rHDL are required in foam cells grown in 2D atheroma model to achieve similar cholesterol efflux concentrations in those cultured in 1D.

Being lipid-poor apoA-I the most efficient acceptor of cholesterol from macrophages in the arterial wall via ABCA1 its effects as cholesterol acceptor was also determined. As shown in Figure S4 in the Supporting Information, cholesterol efflux to apoA-I (10 μg mL^{-1}) in foam cells treated with empty-rHDL was 15.4 ± 1.2%, in the presence of TO901317 was 21.5 ± 2.1%, when cells were pre-treated with antagomiR-33a-loaded rHDL cholesterol efflux was 27.0 ± 1.4%, and combination of TO901317 and antagomiR-33a-loaded rHDL caused a cholesterol efflux to apoA-I of 37.0 ± 2.8%. These results support that antagomir-33a-loaded rHDLs induce ABCA1 in functional level.

3. Discussion

Atherosclerotic plaque formation is a complex process in which macrophages play a key role in progression or regression of plaques.[1] During the last decades, disease management has improved significantly,[58] however research must now shift toward the necessity to develop new therapeutic strategies focused on accelerating atherosclerosis regression.[1] Although animal models provide essential information for atherosclerosis research, 2D culture and 3D multicellular atherosclerosis models allow mimicking in vivo-like conditions,[53,59] tackling the interaction between different cells in atherosclerotic plaques and, understanding the dynamics of new therapeutic approaches. Over the past five years, bionanomaterial-based strategies have emerged as therapeutic or theranostic agents for managing atherosclerosis.[60] Several nanoplatforms to direct delivery of pharmaceutical agents to atherosclerotic plaque-associated macrophages have shown to beneficially modulate disease process and improve outcomes. In example, core–shell nanoplatform composed of a poly(D,L-lactide-*co*-glycolide) efficiently deliver both siRNA against lectin-like oxidized low-density lipoprotein receptor-1 and atorvastatin to the atherosclerotic lesions and, exert a synergistic therapeutic effect on both endothelial cells and macrophages.[61] Similarly, mannose-functionalized dendrimeric nanoparticle (mDNP)-based platforms have been successfully

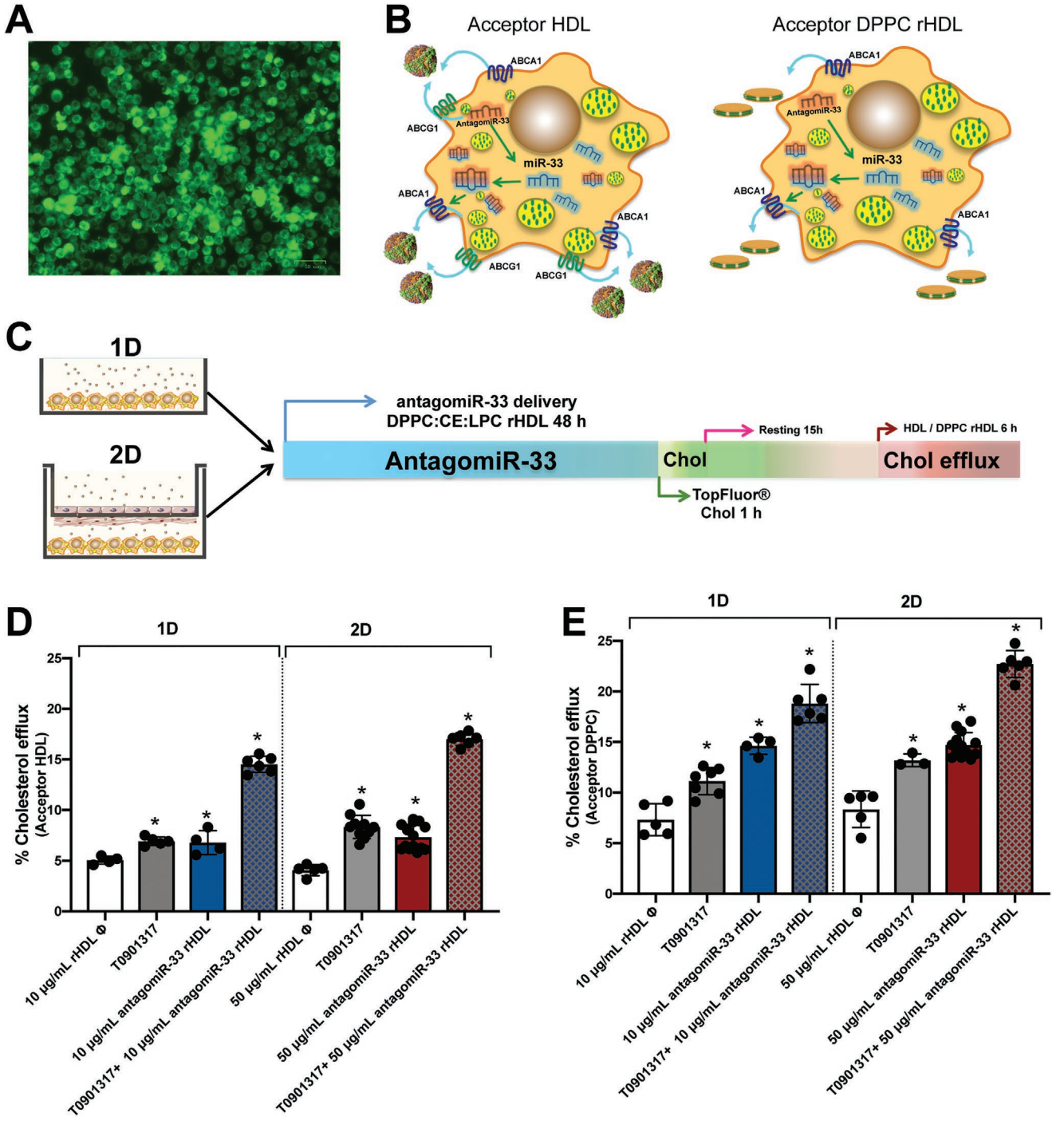

Figure 6. Cholesterol efflux promoted in foam cells by sequential rHDL administration in a triple cell 2D atheroma model. A) Macrophage-derived foam cells loaded with TopFluor Cholesterol. B) Illustration of the acceptors used for cholesterol efflux. C) Schematic representation of time-course sequential administration of rHDL prior cholesterol efflux assay. D) Cholesterol efflux in 1D and 2D atheroma model cultured foam cells with HDL as acceptor. E) Cholesterol efflux in 1D and 2D atheroma model cultured foam cells with DPPC rHDL as acceptor. Cholesterol efflux was calculated as described in the Experimental Section. The data in (D) and (E) represent the mean ± SD of at least three independent measurements. Levels of significance were determined by ANOVA. * $p < 0.01$.

used for macrophage-specific delivery of LXR-L, leading to plaque attenuation and favorable modulation of plaque characteristics.[62] Moreover, mDNPS have also been proven to simultaneously deliver SR-A siRNA (to reduce LDL uptake) and LXR ligand (LXR-L, to stimulate cholesterol efflux) with significant regression of atherosclerotic lesions.[63]

In addition, nanoparticles have turned out to be powerful delivery vehicles for miRNA-based therapeutics through inhibition

of targets that drive disease progression or overexpression of beneficial intermediates in CVD settings.[64–66]

In this work we sought to develop a targeted nanoparticle approach based in a staged administration of rHDL carrying antagomiR-33a to upregulate ABCA1 transporter followed by DPPC rHDL, which has been previously shown to be highly efficient removing cholesterol from foam cells.[40] We have investigated the efficiency of this strategy in a three-cell type 2D culture model mimicking the atheroma plaque microenvironment. A major challenge to realizing this goal has been an effective formulation and delivery of therapeutic miRNAs to the cytoplasm of foam cells in the atheroma context. A conceptual breakthrough to this problem is surpassed with the demonstration that natural HDL contain miRNAs and that these HDL-bound miRNAs have improved stability compared with naked miRNAs.[67] In addition, and taking the advantage that HDLs bind with their high-affinity receptor, scavenger receptor type B1 (SR-B1), we have developed functional HDL-like nanoparticles composed of DPPC:CE:LPC, which physically and chemically resemble to a natural mature HDLs; contain apoA-I, which is the main protein constituent of HDLs,[68] selectively target cells that express SR-B1;[69,70] and show no cytotoxicity (data not shown). Furthermore, HDL-mediated delivery of miRNAs to recipient cells was demonstrated to be dependent on SR-B1.[67] Purified DPPC:CE:LPC rHDLs showed an average diameter of ≈10 nm as determined by DLS and NS-EM and high α-helical structure content determined by CD, indicating a correct reconstitution of rHDLs (Figure 2). In addition, they bound efficiently miRNA, reaching a maximum capacity at 1:1 mol:mol ratio and proved to be very avidly internalized by foam cells in the 2D atheroma model (Figures 3 and 4). It has been reported that HDL-miRNAs are taken up by HDL's receptor, SR-B1 and that transendothelial transport of HDL is actively regulated by a process that involves at least SR-B1, endothelial lipase and ABCG1.[67,71,72] Therefore, and using a transwell system, we tested whether DPPC:CE:LPC rHDL are efficiently transported through EC/VSMC bilayer (Figure 4C,D). Using fluorescent microscopy, we found DiI-rHDL within the ECs and not between the intercellular spaces, confirming the results obtained by others.[73,74] VSMC showed residual intracellular uptake of DiI-labeled DPPC:CE:LPC rHDL while the uptake in macrophage-derived foam cells resulted to be highly efficient (Figure 4C), results that were further corroborated by flow cytometry (Figure 4D). We have also addressed the efficiency of nanoparticles reaching target cells in the 2D atheroma model and found that a fivefold higher concentration is required to achieve similar results than those observed in foam cells cultured alone in monolayer (Figure 5A and Figure S1, Supporting Information).

We found that a simple treatment of DPPC:CE:LPC rHDL-antagomiR-33a for 48 h efficiently reduced intracellular miR-33 leading to upregulation of ABCA1 and ABCG1 transporters (Figure 5). Besides, our results confirm that miRNAs delivered via rHDL can escape the endosomal system and function in the RNA-induced silencing complex complex. Similar results have been shown using PEGylated chitosan nanoparticles delivering antagomiR-33 into the atheroma plaque.[51]

Once the first part of our goal proven to be effective, we further sought to improve the therapeutic relevance of our model by potentiating the extent of cholesterol efflux by a second-step administration of DPPC rHDL. We have previously shown that DPPC rHDL are more efficient favoring cholesterol efflux than CSL-112, nanoparticles composed of soy-PC, which are currently being tested in humans.[40,75] Therefore, and after inducing ABCA1 overexpression by DPPC:CE:LPC rHDL carrying antagomiR-33a, cells were loaded with fluorescent cholesterol and incubated with DPPC rHDL to promote cholesterol efflux (Figure 6). We used two cholesterol acceptors, HDL and DPPC rHDL and compared the efflux efficiency to each acceptor both in foam cells cultured alone and in those cultured in the 2D atheroma model. Cholesterol efflux into mature HDL particles is mainly mediated by ABCG1 transporter while ABCA1 targets mainly lipid free apoA-1 or discoidal pre-β-HDL (DPPC rHDL in our experimental conditions).[40,76,77] We determined similar cholesterol efflux in the foam cells cultured in 1D or in the 2D atheroma model using 10 or 50 μg mL^{-1} of antagomiR-33-loaded DPPC:CE:LPC rHDL, respectively. When HDL was used as cholesterol acceptor, both antagomiR-33a delivery and T0901317 promoted a significant enhanced cholesterol efflux compared to that of cells treated with empty DPPC:CE:LPC (Figure 6D). Being ABCG1 the transporter that mainly mediates cholesterol transport to assembled HDL,[78,79] the results presented here indicate that enhancing the in vitro expression of ABCG1 by delivery of antagomiR-33a is as effective as T0901317 in contributing to cholesterol efflux to HDL. The undesired side-effects of treatments with T0901317, which are associated with enhanced lipogenesis, resulting in elevated serum triglyceride levels and hepatic steatosis, highlights the potential of delivering antagomiR-33a to upregulate ABCG1 and potentiating cholesterol efflux without affecting cell citotoxicity.[80,81] As previously shown, DPPC rHDL-induced cholesterol efflux was more efficient than HDL.[40] Very interestingly, in 1D cultures, cholesterol efflux in cells pretreated with antagomiR-33a-loaded rHDL was two times higher than that in cells treated with empty DPPC:CE:LPC rHDL and slightly but significantly higher than cells treated with TO901317 (Figure 6E). Similarly, in 2D atheroma model, pretreatment with antagomiR-33a-loaded rHDL caused a 1.8 times higher cholesterol efflux compared to cells treated with empty rHDL and slightly higher than cells treated with TO901317 (Figure 6E). These results indicate that using rHDL as antagomiR-33a carrier is an efficient tool to upregulate ABCA1 and its potency is higher than that of T0901317. The higher efficacy of DPPC rHDL compared to natural HDL is in agreement with the study conducted by Adorni et al. showing that ABCA1 accounts for cholesterol efflux of 50%, while approximately 20% of the cholesterol efflux can be attributable to ABCG1.[76]

Notably, the results obtained in this proposed two-step atheroma plaque-targeting strategy highlights its use as a promising therapeutic intervention for favoring reverse cholesterol transport. It also can improve the overall targeted delivery efficiency of rHDL broadening potential applications in several diseases. Bringing the strategy of sequential administration of rHDL into in vivo usage is a challenge that requires further studies before clinical steps can be initiated. Systematic basic studies as those presented here concerning the mechanisms of nanoparticle transport, their interactions with cells and efficacy, improve the translation of basic research into developing

and bringing novel nanomedical tools. This process involves multidisciplinary efforts and requires strong expertise in safety and healthcare issues. As mentioned above, a large number of studies have used rHDL as therapeutic agent addressing the central antiatherogenic and cardioprotective properties of HDL.[56,82] Inflammatory and atherogenic processes have been shown to be reduced by repeated infusion treatment with rHDL.[83] Therefore, sequential administration of antagomiR-33a-loaded rHDL followed by DPPC rHDL infusion could represent a good strategy to favor the reverse transport of cholesterol and contribute to the reduction of atheroma plaque. In any case, future in vivo studies in animal models will provide the necessary information to calculate the doses, the time interval between infusions and determine the antiatherogenic effects of the treatment strategy proposed in this work.

4. Conclusion

In summary, our findings demonstrate that sequential targeting of foam cells with nanoparticles including a first antagomiR-33a delivery by DPPC:CE:LPC rHDL followed by a second infusion of DPPC rHDL induces a potent cholesterol efflux from foam cells, which may overcome current technique barriers to promote clinical applications. Additionally, the usefulness of 2D cell culture models as an experimental approach to bioengineer atheroma models is endorsed by the possibility of dissecting separately the events occurring in the process to better understand the observed effects.

5. Experimental Section

Materials: DPPC, LPC, cholesterol (Chol), and 23-(dipyrrometheneboron difluoride)-24-norcholesterol (TopFluor Cholesterol) were purchased from Avanti Polar Lipids (Alabaster, Alabama, USA).

Cholesteryl linoleate (18:2 CE), sodium cholate hydrate, methyl-β-cyclodextrin, bovine serum albumin (BSA), BSA fatty acid free, acyl-CoA:cholesterol acyltransferase (ACAT) inhibitor (Sandoz 58-035), and cell culture reagents were obtained from Sigma-Aldrich (Madrid, Spain). The synthetic LXR ligand T0901317 was purchased from Cayman Chemical (Ann Arbor, Michigan, USA).

Human ApoA-I Purification: Human apoA-I was purified from *E. coli* BL21 (DE3) pLysS transformed with recombinant hapoA-I (rhapoA-I) vector (kindly provided by Prof. Oda, Children's Hospital Oakland Research Institute (Oakland, CA, USA) as described before.[84] Briefly, protein expression was induced with isopropyl β-D-thiogalactopyranoside (final concentration 0.4×10^{-3} M) in transformed *E. coli* BL21 (DE3) pLysS. Bacteria were maintained for 3 h at 37 °C and then harvested and centrifuged at 6000 × *g* for 15 min at 4 °C. Bacteria pellet was resuspended in protein extraction buffer (20×10^{-3} M Tris-HCl, pH 8.0) supplemented with 0.1% (v/v) IGEPAL CA-630 and protease inhibitors (Complete ethylenediaminetetraacetic acid (EDTA)-free and phenylmethylsulfonyl fluoride 1:100 (v/v)) and sonicated at 4 °C. Samples were centrifuged at 9500 × *g* for 30 min at 4 °C and the supernatant was filtered through 0.2 µm filters and loaded into a HiTrap TALON crude 5 mL (GE Healthcare, Chicago, IL, USA). Protein was eluted in 20×10^{-3} M $NaPO_4$, 500×10^{-3} M NaCl, 500×10^{-3} M imidazole, pH 7.4 after being washed in 20×10^{-3} M $NaPO_4$, 500×10^{-3} M NaCl, 20×10^{-3} M imidazole buffer, pH 7.4. Endotoxin was removed by washing in washing buffer supplemented with Triton X-114 0.1% (v/v). Concentration of apoA-I was determined from its extinction coefficient 32 430 M^{-1} cm^{-1} at 280 nm.

rHDL Reconstitution and Purification: HDL reconstitution was performed as previously described.[40] Briefly, dried lipid mixtures of DPPC or DPPC:CE:LPC (75:20:5% mol), final concentration 12.5×10^{-3} M, were resuspended in Tris-Cl, EDTA, NaCl (TEN) buffer (10×10^{-3} M Tris-HCl, 1×10^{-3} M EDTA, 150×10^{-3} M NaCl, pH 8.0) and vortexed at 42 °C to allow multilamellar vesicle (MLV) formation. Next, sodium cholate was added in 1:1.2 (lipid:cholate) molar ratio to partially solubilize MLVs. As soon as cholate is added, the sample is vortexed and incubated for 5 min at 42 °C (the cycle of vortexing and incubating the sample at 42 °C is repeated three times).

Next, purified apoA-I was added, apoA-I to lipid molar ratio of 1:125 (mol/mol), and the solution was maintained above lipid transition temperature (T_m) for 15 min and mixed vigorously every 5 min. Samples were then incubated overnight at 42 °C and 800 rpm in an Eppendorf Thermomixer (Eppendorf AG, Hamburg, Germany). At the end of the incubation, nanodisc solution was transferred to a cellulose dialysis membrane (14 kDa molecular weight cutoff) (Sigma-Aldrich, Sant Luis, MO, USA) and dialyzed against 5 L of TEN buffer to remove cholate. Dialysis was performed at 42 °C for 48 h, with buffer changing every 24 h. Finally, dialyzed nanodiscs were collected and centrifuged at 13 100 × *g* for 30 min to discard aggregates. Supernatant was then passed through a 0.2 µm filter and maintained at 4 °C.

rHDL purification was performed on a Superdex 200 10/300 GLASS (GE Healthcare, Chicago, IL, USA) with TEN buffer as eluent. The column was calibrated with molecular size standards from Amersham Biosciences (Amersham, UK). Samples were eluted at 4 °C at a 0.2 mL min^{-1} flow rate and elution profiles were expressed as retention volume.

rHDL Characterization: *Circular Dichroism*: Secondary structure content of apoA-I was determined in a thermostatized Jasco 810 spectropolarimeter in a 0.1 cm path length quartz cuvette. Spectra (200–260 nm) were obtained at 25 °C with a bandwidth of 1 nm and response time of 1 s and 50 nm per scan speed. Each spectrum represents the average of 15 accumulations and was corrected subtracting the buffer spectra. Next, for each wavelength, θ_{MRE} (mean residue ellipticity) was calculated using the following formula

$$\theta_{MRE} = \frac{MRW \times DEG/1000}{10 \times [\text{apoA-I}] \times \text{bandwidth}} \quad (1)$$

where MRW = MW/(aa-1); [apoA-I] is the protein concentration (g mL^{-1}); bandwidth is in cm; MW is the molecular weight; aa is the number of amino acids.

The α-helicity of the protein for each rHDL composition was calculated using θ_{MRE} at 222 nm using the following equation: % α-helix = $((\theta)_{222} + 3000)/(36\,000 + 3000) \times 100$.[85]

DLS: The hydrodynamic radius of rHDLs was determined by DLS in a Nano-S Zetasizer (Malvern Instruments, Malvern, UK) as previously described.[86] Measurements were performed in triplicate (15 runs, 10 s each) at 25 °C. Viscosity and refractive index of TEN buffer were applied to the measurements. Data were analyzed using Zetasizer software.

NS-EM: Size and morphology of the rHDL were determined by adsorbing 10 µL of each rHDL preparation on a glow-discharged thin carbon-coated 300-mesh copper grid (Cu-300CN; Pacific Grid-Tech, San Francisco, CA, USA) as previously described.[87] The excess of solution was removed and the grid was washed three times in deionized water. Then, one drop (≈30 µL) of 1% (w/v) uranyl acetate (pH 4.6) solution was applied and maintained for 1–3 min in the dark before excess stain was removed. Finally, the excess of solution was removed and the sample was air dried at room temperature. Fiji software was used for Feret diameter calculation, longitudinal and transversal diameters measurements and particle size quantification.[88] Individual particles were automatically selected and then checked to remove overlapping or damaged particles. 1600 particle images from images of each rHDL sample were used for the statistical analysis of particle size distribution.

Isolation of Human HDL and LDL: HDLs and LDLs were isolated from human plasma of healthy individuals by ultracentrifugation as previously described.[40] Briefly, blood was collected in EDTA tubes and samples were centrifuged for 10 min at 3000 × *g* and at 4 °C. LDL was purified from

the obtained human plasma by ultracentrifugation by adjusting plasma density with KBr to 1.21 g mL^{-1}), for HDL purification, plasma density was adjusted to 1.4 g mL^{-1}. Two phases were generated by layering cold PBS buffer. The samples were centrifuged at 27 000 rpm for 22 h at 4 °C using the Swinging-Bucket 28.1 rotor. The bands corresponding to LDL and HDL were carefully recovered and lipoproteins were passed through a prebalanced Sephadex G25 gel filtration column (PD-10 desalting column, GE Healthcare, Chicago, IL, USA) to remove KBr. Lipoprotein concentration was measured using the detergent compatible Protein Asssay kit (Bio-Rad, Herculaes, CA, USA).

Lipoprotein size was measured using DLS as described above and polydispersity was analyzed. Samples were stored at 4 °C for a maximum of two weeks. The study was conducted according to the guidelines of the Declaration of Helsinki, and approved by the Institutional Review Board Research Ethics Committee from the University of the Basque Country (Comité de Ética en la Investigación y la Práctica Docente de la Universidad del País Vasco/Euskal Herriko Unibertsitatea, CEID/IIEB).

LDL Acetylation: LDL acetylation was performed as previously described and[40] LDL acetylation was confirmed by 0.7% agarose gel electrophoresis in 90×10^{-3} M Tris-HCl, 80×10^{-3} M boric acid, pH 8.2 buffer (Figure S5, Supporting Information). Detailed methodology can be found in the Supporting Information.

Quantitative and Qualitative Analysis of Foam Cell Formation: Quantitative analysis of the formation of foam cells (acetylated LDL 125 μg mL^{-1}) was performed with Oil-Red-O (ORO) dye (Sigma-Aldrich, Saint Luis, MO, USA) as described before.[40] ORO signal was relativized to cell number by staining the cell nuclei with Crystal Violet (Sigma-Aldrich, Saint Luis, MO, USA) (Figure S6A, Supporting Information).

Qualitative analysis of foam cells was performed by optical microscopy by visualizing lipid droplets with ORO staining and nuclei with Mayer´s Hematoxylin (Sigma-Aldrich, Madrid, Spain). (Figure S6B,C, Supporting Information). Detailed methodology can be found in the Supporting Information.

Cell Cultures: Human umbilical vein endothelial cells (HUVECs) were kindly provided by Dr. Alicia Rodriguez (University of the Basque Country, Universidad del País Vasco/Euskal Herriko Unibertsitatea; Spain) and human artery smooth muscle cells (VSMCs) were purchased from Coriell Cell Repositories (Coriell AG11545, Camden, NJ, USA) and used between passages six and nine for all experiments. Monocultures of all vascular cells were maintained in 75 cm^2 tissue culture treated vented flasks (Corning, Corning, NY, USA) in a 37 °C and 5% CO_2 environment in the appropriate media. For VSMC, flasks were previously coated with 0.1% gelatin (Sigma-Aldrich, Madrid, Spain) and cells were incubated in medium 199 (Thermofisher Scientific, Paisley, UK) supplemented with fetal bovine serum (FBS; Thermo Fisher Scientific, Inchinnan, UK), 0.02 mg mL^{-1} endothelial cell growth supplement, 0.05 mg mL^{-1} Heparin, and 2×10^{-3} M L-glutamine. J774A.1 macrophages were maintained in Dulbecco's modified Eagle medium media (Thermo Fisher Scientific, Paisley, UK) supplemented with 10% FBS (Thermo Fisher Scientific, Inchinnan, UK), L-glutamine (Thermo Fisher Scientific, Inchinnan, UK), and Penicillin/Streptomycin (Sigma Aldrich, Madrid, Spain). Monocultures of J774A.1 cells were maintained in 75 cm^2 tissue culture treated vented flasks (Corning, Corning, NY, USA) in a 37 °C and 5% CO_2 environment. The differentiation of J774A.1 cells to foam cells was achieved by incubating for 24 h the cells with 125 μg mL^{-1} acetylated LDL in 24 well tissue culture treated plates (Corning, Corning, NY, USA).

Atheroma Plaque Model: Triple-Cell Coculture: Development of triple-compartment cell culture 2D model comprising ECs, VSMCs and foam cells mimicking the atheroma plaque components in vitro is illustrated in Figure S7, Supporting Information). VSMCs were seeded at a density of 8×10^4 cells on the underside of 0.1% Gelatin (Sigma-Aldrich, Madrid, Spain) coated 0.4 μm pore 24 well transwell inserts (Corning, Corning, NY, USA). This was achieved by inverting the insert and seeding VSMCs in 50 μL of VSMC media onto the bottom of the insert (Figure S7, Supporting Information). The VSMCs were then allowed to adhere to the transwell membrane for 1 h at 37 °C and 5% CO_2. The transwell was then reoriented and 0.5 mL VSMC media was gently added into the well and 200 μL on top of the insert. The following day, ECs were seeded at confluent density (8×10^4 cells) on the upper surface of the transwell inserts and rested for additional 24 h (Figure S7, Supporting Information). J774A.1 derived foam cells were prepared in separate wells to ensure they were ready for use following the 24 h rest period. In this case, J774A.1 cells were differentiated to foam cells by growing the cells in the presence of 125 μg mL^{-1} acetylated LDL for 24 h in Opti-MEM (Thermofisher Sci., Madrid, Spain).[40] Then, foam cells were washed thoroughly to remove any residual acetylated LDL and wells were filled with medium 199. Coculture inserts were then transferred into wells containing foam cells (Figure S7, Supporting Information).

TEER Measurement: TEER measurement is a noninvasive technique for indirectly evaluating the tight junction integrity of the cells through the measurement of the electrical resistance across a cellular layer. The evaluation of TEER value was performed by using TEER measurement equipment (Millicell ERS-2 Voltohmmeter, Merck, Darmstadt, Germany). The TEER values of transwell membrane and transwell membrane with ECs monolayer were measured in triplicate. The TEER values were finally determined as follows

$$TEER\left(\Omega \cdot cm^2\right) = \left(RT\left(\Omega\right) - RB\left(\Omega\right)\right) \times A\left(cm^2\right) \quad (2)$$

where RT is the total resistance across the cellular monolayer on the membrane, RB is the blank resistance of the membrane only (without cells), and A is the surface area of the membrane (0.33 cm^2 in this 12 well insert case).

Quantification of DiI-Labeled DPPC:CE:LPC rHDL by Flow Cytometry: To determine internalized DiI-labeled DPPC:CE:LPC rHDL by Fluorescent Activated Cell Sorter, cells were incubated with the labeled rHDL for 24 h in the transwell inserts (ECs, VSMC and foam cells) or foam cells cultured alone in monolayer. Then, cells were washed twice with PBS and each cell type was recovered from its compartment by incubating the cells with PBS supplemented with EDTA 5×10^{-3} M. Once detached, fluorescence of 10 000 events was acquired for data analysis. Fluorescence intensities (FI) were measured by flow cytometry on a CytoFlex (Beckman Coulter, Madrid, Spain). All measurements were performed at least in triplicate and 10 000 events were acquired for data analysis in each sample.

MicroRNA Delivery: *rHDL-miRNA Conjugation*: HDL particles in TEN buffer were incubated with miRNAs (Hairpin Inhibitor Control or hsa-miR-33a-5p hairpin inhibitor) for 90 min at 30 °C in agitation. The efficiency of miRNA binding to rHDL was determined by qRT-polymerase chain reaction. rHDL was conjugated to Hairpin Inhibitor Control (based on cel-miR-67 mature sequence) at miRNA:protein mol ratios ranging 0.001–10:1. Samples were next washed four times in the same buffer by centrifugation (Amicon Ultra-4 Centrifugal Filter Units (100 000 Dalton Pores, Merck, Darmstadt Germany)) and TRIzol reagent (Thermofisher Sci., Madrid, Spain) was used for extraction and purification following the manufacturer's guidelines. 20 pmol UniSp6 spike-in RNA (QIAGEN, Germany) were added to each sample for extraction control and normalization. To quantify bound miRNA, miRCURY locked nucleic acid miRNA PCR System (QUIAGEN, Germany) was used on a CFX96 Touch Real-Time PCR Detection System (Bio-Rad, CA, USA) according to manufacturer's protocol. cel-miR-67 miRCURY LNA miRNA PCR Assay (QIAGEN, Germany) that matched the mature form of miRNA cel-miR-67–3p was used as primers.

miRNA Delivery and Functional Studies: For assay optimization, conjugated rHDLs with miRNA at 1:1 miRNA:protein mol ratio were diluted in Opti-MEM (Thermofisher Sci., Madrid, Spain) (0–20 μg mL^{-1} of protein in foam cell monolayers or 0–100 μg mL^{-1} in the ECs compartment in 2D cultures) and incubated 24 h with the cells seeded in 24-well plates. To determine miRNA delivery efficiency and activity, the following day cells were washed twice with PBS and TRIzol reagent was added for total RNA extraction.

For functional studies cells were incubated with miRNA conjugated rHDLs (1:1 miRNA:protein mol ratio) for 24 h in Opti-MEM (Thermofisher Sci., Madrid, Spain). Then, the same volume of DMEM medium (Sigma-Aldrich, Madrid, Spain) supplemented with 20% (v/v) FBS, 2×10^{-3} M L-glutamine (Invitrogen, Madrid, Spain), 100 units mL^{-1} penicillin, and 100 μg mL^{-1} streptomycin (Invitrogen, Madrid, Spain)

was added. After additional 24 h, cells were washed with PBS, and TRIzol reagent was added to determine miRNA and mRNA levels, or lysis buffer (50×10^{-3} M Tris-HCl, pH 7.5, 0.1% sodium dodecyl sulphate, 0.1% deoxycholic acid, 0.1×10^{-3} M EDTA, 0.1×10^{-3} M Ethylene glycol tetraacetic acid, 1% NP-40, 5.3×10^{-3} M NaF and 1.5×10^{-3} M NaP) to determine protein levels.

RNA Isolation and Quantitative Real-Time PCR: For mRNA and miRNA quantification, total RNA from cells was isolated using TRIzol reagent according to manufacturer's guidelines. For *ABCA1* and *ABCG1* mRNA expression study, One Step SYBR PrimeScript RT-PCR Kit (Perfect Real Time) (Takara, Japan) was used for cDNA synthesis and quantitative PCR. Glyceraldehyde 3-phosphate dehydrogenase mRNA was used as the housekeeping mRNA for normalization. For miRNA analysis, miRCURY LNA miRNA PCR System (QUIAGEN, Germany) was used as before. U6 snRNA was used as the housekeeping control for normalization. All primers were synthesized (Laboratorios Conda, Spain) based on sequences published in Massachusetts General Hospital PrimerBank (https://pga.mgh.harvard.edu/primerbank/).

Cholesterol Efflux Assay: Functionality of rHDLs was analyzed through their capacity to induce cholesterol efflux from cells loaded with TopFluor-Cholesterol as described before.[40] Labeling medium was prepared by complexing a mixture of cholesterol and TopFluor-cholesterol (3:1, M:M) with β-cyclodextrin (16×10^{-3} M). Once mixed, cholesterol was dried under nitrogen stream and mixed with an 80-molar excess of β-cyclodextrin dissolved in minimum essential medium eagle (MEM)-Hepes 25×10^{-3} M media (pH 7.4). Finally, the mixture was sonicated at 40 °C in a water bath for 30 min to resuspend cholesterol and further incubated for 3 h at 37 °C in agitation.

After antagomiR-33a delivery by DPPC:CE:LPC rHDL across 2D cocultures (Figure S8, Supporting Information), macrophage-differentiated foam cells were loaded with labeling media diluted in Roswell Park Memorial Institute Medium-1640 containing 0.4% BSA and 4 μg mL^{-1} ACAT inhibitor (1:1, v:v) plus 2% of FBS, for an hour. Cells were then washed and incubated in RPMI-1640 containing 0.2% BSA and 2 μg mL^{-1} ACAT inhibitor for 15 h with or without 3×10^{-6} M of TO901317 LXR agonist in order to induce ABCA1 and ABCG1 upregulation.[57]

After resting time, DPPC rHDLs or HDLs were added to the cells in MEM-Hepes 25×10^{-3} M (pH 7.4) containing 2 μg mL^{-1} ACAT inhibitor. As an internal control of the experiment, BSA 10 μg mL^{-1} was added to TopFluor-Cholesterol loaded cells to obtain nonspecific efflux in the absence of acceptors. After 6 h incubation, media and cells were collected to assess cholesterol efflux.

Since nanoparticles were reconstituted using human recombinant apoA-I and cholesterol efflux was assessed in murine macrophages, purified human recombinant apoA-I was used to determining specific efflux from ABCA1 transporter. It has been previously demonstrated that the ABCA1-mediated efflux of free cholesterol from ABCA1-expressing J774.A1 cells exhibits a hyperbolic dependence on the concentration of human apoA-I in the extracellular medium and conforms to the Michaelis–Menten equation similar to that of mouse apoA-I.[89] In addition, it has been shown that efflux to recombinant human apoA-I and human plasma apoA-I is similar.[90]

Collected media were centrifuged for 15 min at 2900 × *g* to remove cell debris. Cell monolayers were washed gently with MEM-Hepes 25×10^{-3} M and solubilized with lysis buffer (50×10^{-3} M Tris-HCl, pH 7.5, 0.1% SDS, 0.1% deoxycholic acid, 0.1×10^{-3} M EDTA, 0.1×10^{-3} M EGTA, 1% NP-40, 5.3×10^{-3} M NaF, and 1.5×10^{-3} M NaP) during 30 min in a plate shaker at room temperature. Fluorescence of both culture media and cell lysates was measured using a Synergy HTX Multimode microplate reader (λ_{ex}: 485 ± 20 nm, λ_{em}: 528 ± 20 nm) and FI were used to calculate cholesterol efflux in each condition as follows

$$\text{Cholesterol efflux}\,\% = \frac{\text{culture media FI}}{\text{culture media FI} + \text{cell lysate FI}} \times 100 \quad (3)$$

Culture media FI was obtained by subtracting the fluorescence intensity of the media with no acceptors. Specific efflux of each acceptor was calculated by subtracting the efflux to BSA.

Statistical Analysis: All measurements were performed at least three times, unless otherwise stated, and results are presented as mean ± standard deviation. A Shapiro–Wilk test was performed to confirm that the data were normally distributed. The null hypothesis was verified, indicating that the data were normally distributed. For the statistical analysis of variables with a normal distribution, the Student *t*–test or Analysis of variance was used. The categorical variables were compared using the Chi square test or Fisher's exact test. A *p*-value <0.05 was considered significant. All statistical analyzes were performed with the SPSS 25 (SPSS, Inc., Chicago, IL, USA).

Supporting Information

Supporting Information is available from the Wiley Online Library or from the author.

Acknowledgements

This work was supported by Ministerio De Ciencia e Innovación; Proyectos De Generación De Conocimiento 2021 (Ref: PID2021-127056OB-I00). U.G.-G. was supported by Fundación Biofísica Bizkaia. A.B.-V. was supported by Programa de especialización de Personal Investigador Doctor en la UPV/EHU (2019) 2019–2020. S.J.-B. and A.L.-S. were supported by a grant Programa Investigador en Formación (2017–2018) and (2019–2020), Gobierno Vasco, respectively. A.L.-S. was partially supported by Fundación Biofísica Bizkaia. The authors sincerely thank Richard Murray (Fundación Biofísica Bizkaia) for his critical reading and editing of this paper.

Conflict of Interest

The authors declare no conflict of interest.

Data Availability Statement

The data that support the findings of this study are available from the corresponding author upon reasonable request.

Keywords

apoA-I, atherosclerosis models, cardiovascular diseases, cholesterol efflux, microRNAs, nanodiscs, recombinant/reconstituted high-density lipoproteins (rHDL)

Received: September 27, 2021
Revised: December 30, 2021
Published online: February 13, 2022

[1] World Health Organization, *Cardiovascular Diseases (CVDs)* **2020**.
[2] G. K. Hansson, A. Hermansson, *Nat. Immunol.* **2011**, *12*, 204.
[3] P. Libby, *Arterioscler., Thromb., Vasc. Biol.* **2012**, *32*, 2045.
[4] P. Welsh, G. Grassia, S. Botha, N. Sattar, P. Maffia, *Br. J. Pharmacol.* **2017**, *174*, 3898.
[5] I. Tabas, K. J. Williams, J. Boren, *Circulation* **2007**, *116*, 1832.
[6] A. Daiber, S. Steven, A. Weber, V. V. Shuvaev, V. R. Muzykantov, I. Laher, H. Li, S. Lamas, T. Munzel, *Br. J. Pharmacol.* **2017**, *174*, 1591.
[7] J. Davignon, P. Ganz, *Circulation* **2004**, *109*, III27.

[8] S. Verma, M. R. Buchanan, T. J. Anderson, *Circulation* **2003**, *108*, 2054.
[9] K. J. Moore, M. W. Freeman, *Arterioscler., Thromb., Vasc. Biol.* **2006**, *26*, 1702.
[10] A. Benito-Vicente, K. B. Uribe, S. Jebari, U. Galicia-Garcia, H. Ostolaza, C. Martin, *Int. J. Mol. Sci.* **2018**, *19*, 3426.
[11] J. Boren, M. J. Chapman, R. M. Krauss, C. J. Packard, J. F. Bentzon, C. J. Binder, M. J. Daemen, L. L. Demer, R. A. Hegele, S. J. Nicholls, B. G. Nordestgaard, G. F. Watts, E. Bruckert, S. Fazio, B. A. Ference, I. Graham, J. D. Horton, U. Landmesser, U. Laufs, L. Masana, G. Pasterkamp, F. J. Raal, K. K. Ray, H. Schunkert, M. R. Taskinen, B. van de Sluis, O. Wiklund, L. Tokgozoglu, A. L. Catapano, H. N. Ginsberg, *Eur. Heart J.* **2020**, *41*, 2313.
[12] G. Camejo, E. Hurt-Camejo, *J. Lipid Res.* **2014**, *55*, 1.
[13] E. Hurt-Camejo, G. Camejo, *J. Cardiovasc. Dev. Dis.* **2018**, *5*, 1.
[14] R. J. Chilton, *J. Am. Osteopath. Assoc.* **2004**, *104*, S5.
[15] B. A. Ference, H. N. Ginsberg, I. Graham, K. K. Ray, C. J. Packard, E. Bruckert, R. A. Hegele, R. M. Krauss, F. J. Raal, H. Schunkert, G. F. Watts, J. Boren, S. Fazio, J. D. Horton, L. Masana, S. J. Nicholls, B. G. Nordestgaard, B. van de Sluis, M. R. Taskinen, L. Tokgozoglu, U. Landmesser, U. Laufs, O. Wiklund, J. K. Stock, M. J. Chapman, A. L. Catapano, *Eur. Heart J.* **2017**, *38*, 2459.
[16] C. Messier, N. Awad, M. Gagnon, *Neurol. Res.* **2004**, *26*, 567.
[17] M. Cuchel, D. J. Rader, *Circulation* **2006**, *113*, 2548.
[18] A. J. Lusis, *Nature* **2000**, *407*, 233.
[19] T. Moore, A. Le, T. M. Cowan, *J. Inherit. Metab. Dis.* **2012**, *35*, 431.
[20] K. Y. Chyu, P. K. Shah, *Front. Pharmacol.* **2015**, *6*, 187.
[21] C. Michael Gibson, S. Korjian, P. Tricoci, Y. Daaboul, M. Yee, P. Jain, J. H. Alexander, P. G. Steg, A. M. Lincoff, J. J. Kastelein, R. Mehran, D. M. D'Andrea, L. I. Deckelbaum, B. Merkely, M. Zarebinski, T. O. Ophuis, R. A. Harrington, *Circulation* **2016**, *134*, 1918.
[22] P. Barter, A. M. Gotto, J. C. LaRosa, J. Maroni, M. Szarek, S. M. Grundy, J. J. Kastelein, V. Bittner, J. C. Fruchart, *N. Engl. J. Med.* **2007**, *357*, 1301.
[23] D. J. Gordon, J. L. Probstfield, R. J. Garrison, J. D. Neaton, W. P. Castelli, J. D. Knoke, D. R. Jacobs, Jr., S. Bangdiwala, H. A. Tyroler, *Circulation* **1989**, *79*, 8.
[24] J. J. Badimon, L. Badimon, V. Fuster, *J. Clin. Invest.* **1990**, *85*, 1234.
[25] J. A. Shaw, A. Bobik, A. Murphy, P. Kanellakis, P. Blombery, N. Mukhamedova, K. Woollard, S. Lyon, D. Sviridov, A. M. Dart, *Circ. Res.* **2008**, *103*, 1084.
[26] M. J. Amar, W. D'Souza, S. Turner, S. Demosky, D. Sviridov, J. Stonik, J. Luchoomun, J. Voogt, M. Hellerstein, D. Sviridov, A. T. Remaley, *J. Pharmacol. Exp. Ther.* **2010**, *334*, 634.
[27] B. A. Di Bartolo, S. J. Nicholls, S. Bao, K. A. Rye, A. K. Heather, P. J. Barter, C. Bursill, *Atherosclerosis* **2011**, *217*, 395.
[28] R. Duivenvoorden, J. Tang, D. P. Cormode, A. J. Mieszawska, D. Izquierdo-Garcia, C. Ozcan, M. J. Otten, N. Zaidi, M. E. Lobatto, S. M. van Rijs, B. Priem, E. L. Kuan, C. Martel, B. Hewing, H. Sager, M. Nahrendorf, G. J. Randolph, E. S. Stroes, V. Fuster, E. A. Fisher, Z. A. Fayad, W. J. Mulder, *Nat. Commun.* **2014**, *5*, 3065.
[29] C. M. Gibson, J. J. P. Kastelein, A. T. Phillips, P. E. Aylward, M. K. Yee, M. Tendera, S. J. Nicholls, S. Pocock, S. G. Goodman, J. H. Alexander, A. M. Lincoff, C. Bode, D. Duffy, M. Heise, G. Berman, S. J. Mears, P. Tricoci, L. I. Deckelbaum, P. G. Steg, P. Ridker, R. Mehran, *Am. Heart J.* **2021**, *231*, 121.
[30] C. R. Sirtori, L. Calabresi, G. Franceschini, D. Baldassarre, M. Amato, J. Johansson, M. Salvetti, C. Monteduro, R. Zulli, M. L. Muiesan, E. Agabiti-Rosei, *Circulation* **2001**, *103*, 1949.
[31] V. Gualandri, G. Franceschini, C. R. Sirtori, G. Gianfranceschi, G. B. Orsini, A. Cerrone, A. Menotti, *Am. J. Hum. Genet.* **1985**, *37*, 1083.
[32] S. E. Nissen, T. Tsunoda, E. M. Tuzcu, P. Schoenhagen, C. J. Cooper, M. Yasin, G. M. Eaton, M. A. Lauer, W. S. Sheldon, C. L. Grines, S. Halpern, T. Crowe, J. C. Blankenship, R. Kerensky, *JAMA* **2003**, *290*, 2292.
[33] J. A. A. Reijers, D. G. Kallend, K. E. Malone, J. W. Jukema, P. L. J. Wijngaard, J. Burggraaf, M. Moerland, *Cardiovasc. Drugs Ther.* **2017**, *31*, 381.
[34] S. J. Nicholls, R. Puri, C. M. Ballantyne, J. W. Jukema, J. J. P. Kastelein, W. Koenig, R. S. Wright, D. Kallend, P. Wijngaard, M. Borgman, K. Wolski, S. E. Nissen, *JAMA Cardiol.* **2018**, *3*, 806.
[35] J. C. Tardif, C. M. Ballantyne, P. Barter, J. L. Dasseux, Z. A. Fayad, M. C. Guertin, J. J. Kastelein, C. Keyserling, H. Klepp, W. Koenig, P. L. L'Allier, J. Lesperance, T. F. Luscher, J. F. Paolini, A. Tawakol, D. D. Waters, *Eur. Heart. J.* **2014**, *35*, 3277.
[36] J. C. Tardif, J. Gregoire, P. L. L'Allier, R. Ibrahim, J. Lesperance, T. M. Heinonen, S. Kouz, C. Berry, R. Basser, M. A. Lavoie, M. C. Guertin, J. Rodes-Cabau, *JAMA* **2007**, *297*, 1675.
[37] R. Easton, A. Gille, D. D'Andrea, R. Davis, S. D. Wright, C. Shear, *J. Clin. Pharmacol.* **2014**, *54*, 301.
[38] C. I. Ma, J. A. Beckstead, A. Thompson, A. Hafiane, R. H. Wang, R. O. Ryan, R. S. Kiss, *Biochem. Cell Biol.* **2012**, *90*, 636.
[39] P. Marmillot, S. Patel, M. R. Lakshman, *Metabolism* **2007**, *56*, 251.
[40] S. Jebari-Benslaiman, K. B. Uribe, A. Benito-Vicente, U. Galicia-Garcia, A. Larrea-Sebal, I. Alloza, K. Vandenbroeck, H. Ostolaza, C. Martin, *Biomedicines* **2020**, *8*, 373.
[41] P. D. Thomas, M. J. Poznansky, *Biochem. J.* **1988**, *254*, 155.
[42] D. A. Bricarello, J. T. Smilowitz, A. M. Zivkovic, J. B. German, A. N. Parikh, *ACS Nano* **2011**, *5*, 42.
[43] S. I. Kim, D. Shin, T. H. Choi, J. C. Lee, G. J. Cheon, K. Y. Kim, M. Park, M. Kim, *Mol. Ther.* **2007**, *15*, 1145.
[44] H. Lee, S. I. Kim, D. Shin, Y. Yoon, T. H. Choi, G. J. Cheon, M. Kim, *Biochem. Biophys. Res. Commun.* **2009**, *378*, 192.
[45] K. J. Rayner, F. J. Sheedy, C. C. Esau, F. N. Hussain, R. E. Temel, S. Parathath, J. M. van Gils, A. J. Rayner, A. N. Chang, Y. Suarez, C. Fernandez-Hernando, E. A. Fisher, K. J. Moore, *J. Clin. Invest.* **2011**, *121*, 2921.
[46] V. Rottiers, S. Obad, A. Petri, R. McGarrah, M. W. Lindholm, J. C. Black, S. Sinha, R. J. Goody, M. S. Lawrence, A. S. deLemos, H. F. Hansen, S. Whittaker, S. Henry, R. Brookes, S. H. Najafi-Shoushtari, R. T. Chung, J. R. Whetstine, R. E. Gerszten, S. Kauppinen, A. M. Naar, *Sci. Transl. Med.* **2013**, *5*, 212ra162.
[47] N. L. Price, L. Goedeke, Y. Suarez, C. Fernandez-Hernando, *EMBO Mol. Med.* **2021**, *13*, e12606.
[48] L. He, G. J. Hannon, *Nat. Rev. Genet.* **2004**, *5*, 522.
[49] D. Baek, J. Villen, C. Shin, F. D. Camargo, S. P. Gygi, D. P. Bartel, *Nature* **2008**, *455*, 64.
[50] A. T. Ashizawa, J. Cortes, *Expert Opin. Drug Delivery* **2015**, *12*, 1107.
[51] M. A. Nguyen, H. Wyatt, L. Susser, M. Geoffrion, A. Rasheed, A. C. Duchez, M. L. Cottee, E. Afolayan, E. Farah, Z. Kahiel, M. Cote, S. Gadde, K. J. Rayner, *ACS Nano* **2019**, *13*, 6491.
[52] M. C. Zuniga, S. L. White, W. Zhou, *Vasc. Med.* **2014**, *19*, 394.
[53] J. Noonan, G. Grassia, N. MacRitchie, P. Garside, T. J. Guzik, A. C. Bradshaw, P. Maffia, *Front. Immunol.* **2019**, *10*, 849.
[54] D. Kim, S. Eom, S. M. Park, H. Hong, D. S. Kim, *Sci. Rep.* **2019**, *9*, 14915.
[55] W. Tschugguel, Z. Zhegu, L. Gajdzik, M. Maier, B. R. Binder, J. Graf, *Pflugers Arch.* **1995**, *430*, 145.
[56] K. B. Uribe, A. Benito-Vicente, C. Martin, F. Blanco-Vaca, N. Rotllan, *Biomater. Sci.* **2021**, *9*, 3185.
[57] C. M. Ramirez, C. S. Lin, K. Abdelmohsen, L. Goedeke, J. H. Yoon, J. Madrigal-Matute, J. L. Martin-Ventura, D. T. Vo, P. J. Uren, L. O. Penalva, M. Gorospe, C. Fernandez-Hernando, *J. Lipid Res.* **2014**, *55*, 1066.
[58] P. Libby, J. E. Buring, L. Badimon, G. K. Hansson, J. Deanfield, M. S. Bittencourt, L. Tokgozoglu, E. F. Lewis, *Nat. Rev. Dis. Primers* **2019**, *5*, 56.
[59] D. F. Gualtero, G. I. Lafaurie, M. R. Fontanilla, *Mol. Oral. Microbiol.* **2018**, *33*, 29.

[60] C. K. W. Chan, L. Zhang, C. K. Cheng, H. Yang, Y. Huang, X. Y. Tian, C. H. J. Choi, *Small* **2018**, *14*, 1702793.
[61] Y. Zhao, H. Gao, J. He, C. Jiang, J. Lu, W. Zhang, H. Yang, J. Liu, *J. Controlled Release* **2018**, *283*, 241.
[62] H. He, Q. Yuan, J. Bie, R. L. Wallace, P. J. Yannie, J. Wang, M. G. Lancina, 3rd, O. Y. Zolotarskaya, W. Korzun, H. Yang, S. Ghosh, *Transl. Res.* **2018**, *193*, 13.
[63] H. He, J. Wang, P. J. Yannie, W. J. Korzun, H. Yang, S. Ghosh, *Biomaterials* **2020**, *260*, 120333.
[64] J. E. Dahlman, C. Barnes, O. Khan, A. Thiriot, S. Jhunjunwala, T. E. Shaw, Y. Xing, H. B. Sager, G. Sahay, L. Speciner, A. Bader, R. L. Bogorad, H. Yin, T. Racie, Y. Dong, S. Jiang, D. Seedorf, A. Dave, K. S. Sandu, M. J. Webber, T. Novobrantseva, V. M. Ruda, A. K. R. Lytton-Jean, C. G. Levins, B. Kalish, D. K. Mudge, M. Perez, L. Abezgauz, P. Dutta, L. Smith, et al., *Nat. Nanotechnol.* **2014**, *9*, 648.
[65] H. Yin, R. L. Kanasty, A. A. Eltoukhy, A. J. Vegas, J. R. Dorkin, D. G. Anderson, *Nat. Rev. Genet.* **2014**, *15*, 541.
[66] O. F. Khan, P. S. Kowalski, J. C. Doloff, J. K. Tsosie, V. Bakthavatchalu, C. B. Winn, J. Haupt, M. Jamiel, R. Langer, D. G. Anderson, *Sci. Adv.* **2018**, *4*, eaar8409.
[67] K. C. Vickers, B. T. Palmisano, B. M. Shoucri, R. D. Shamburek, A. T. Remaley, *Nat. Cell Biol.* **2011**, *13*, 423.
[68] C. S. Thaxton, J. S. Rink, P. C. Naha, D. P. Cormode, *Adv. Drug Delivery Rev.* **2016**, *106*, 116.
[69] J. S. Rink, S. Yang, O. Cen, T. Taxter, K. M. McMahon, S. Misener, A. Behdad, R. Longnecker, L. I. Gordon, C. S. Thaxton, *Mol. Pharm.* **2017**, *14*, 4042.
[70] S. Yang, M. G. Damiano, H. Zhang, S. Tripathy, A. J. Luthi, J. S. Rink, A. V. Ugolkov, A. T. Singh, S. S. Dave, L. I. Gordon, C. S. Thaxton, *Proc. Natl. Acad. Sci. U. S. A.* **2013**, *110*, 2511.
[71] J. Robert, M. Lehner, S. Frank, D. Perisa, A. von Eckardstein, L. Rohrer, *Arterioscler. Thromb. Vasc. Biol.* **2013**, *33*, 2699.
[72] L. Rohrer, P. M. Ohnsorg, M. Lehner, F. Landolt, F. Rinninger, A. von Eckardstein, *Circ. Res.* **2009**, *104*, 1142.
[73] D. Perisa, L. Rohrer, A. Kaech, A. von Eckardstein, *Biochim. Biophys. Acta* **2016**, *1861*, 98.
[74] K. Y. Fung, C. Wang, S. Nyegaard, B. Heit, G. D. Fairn, W. L. Lee, *Front. Physiol.* **2017**, *8*, 841.
[75] S. Sankaranarayanan, J. F. Oram, B. F. Asztalos, A. M. Vaughan, S. Lund-Katz, M. P. Adorni, M. C. Phillips, G. H. Rothblat, *J. Lipid Res.* **2009**, *50*, 275.
[76] M. P. Adorni, F. Zimetti, J. T. Billheimer, N. Wang, D. J. Rader, M. C. Phillips, G. H. Rothblat, *J. Lipid Res.* **2007**, *48*, 2453.
[77] A. R. Tall, *J. Intern. Med.* **2008**, *263*, 256.
[78] M. A. Kennedy, G. C. Barrera, K. Nakamura, A. Baldan, P. Tarr, M. C. Fishbein, J. Frank, O. L. Francone, P. A. Edwards, *Cell Metab.* **2005**, *1*, 121.
[79] K. Nakamura, M. A. Kennedy, A. Baldan, D. D. Bojanic, K. Lyons, P. A. Edwards, *J. Biol. Chem.* **2004**, *279*, 45980.
[80] J. J. Repa, G. Liang, J. Ou, Y. Bashmakov, J. M. Lobaccaro, I. Shimomura, B. Shan, M. S. Brown, J. L. Goldstein, D. J. Mangelsdorf, *Genes. Dev.* **2000**, *14*, 2819.
[81] G. Liang, J. Yang, J. D. Horton, R. E. Hammer, J. L. Goldstein, M. S. Brown, *J. Biol. Chem.* **2002**, *277*, 9520.
[82] C. R. Sirtori, L. Calabresi, G. Franceschini, *Atherosclerosis* **1999**, *142*, 29.
[83] A. Murphy, J. Chin-Dusting, D. Sviridov, *Clin. Lipidol.* **2009**, *4*, 731.
[84] G. Cavigiolio, B. Shao, E. G. Geier, G. Ren, J. W. Heinecke, M. N. Oda, *Biochemistry* **2008**, *47*, 4770.
[85] N. Greenfield, G. D. Fasman, *Biochemistry* **1969**, *8*, 4108.
[86] T. Klemetsrud, H. Jonassen, M. Hiorth, A. L. Kjoniksen, G. Smistad, *Colloids Surf., B* **2013**, *103*, 158.
[87] J. A. Fernandez-Higuero, A. Etxebarria, A. Benito-Vicente, A. C. Alves, J. L. Arrondo, H. Ostolaza, M. Bourbon, C. Martin, *Sci. Rep.* **2015**, *5*, 18184.
[88] J. Schindelin, I. Arganda-Carreras, E. Frise, V. Kaynig, M. Longair, T. Pietzsch, S. Preibisch, C. Rueden, S. Saalfeld, B. Schmid, J. Y. Tinevez, D. J. White, V. Hartenstein, K. Eliceiri, P. Tomancak, A. Cardona, *Nat. Methods* **2012**, *9*, 676.
[89] C. Vedhachalam, P. S. Chetty, M. Nickel, P. Dhanasekaran, S. Lund-Katz, G. H. Rothblat, M. C. Phillips, *J. Biol. Chem.* **2010**, *285*, 31965.
[90] C. Vedhachalam, L. Liu, M. Nickel, P. Dhanasekaran, G. M. Anantharamaiah, S. Lund-Katz, G. H. Rothblat, M. C. Phillips, *J. Biol. Chem.* **2004**, *279*, 49931.